GOLGA2/GM130, *cis*-Golgi Matrix Protein, is a Novel Target of Anticancer Gene Therapy

Seung-Hee Chang[1], Seong-Ho Hong[1], Hu-Lin Jiang[1,2], Arash Minai-Tehrani[1], Kyeong-Nam Yu[1], Jae-Ho Lee[1], Ji-Eun Kim[1,3], Ji-Young Shin[1], Bitna Kang[1], Sungjin Park[1], Kiwon Han[4], Chanhee Chae[4] and Myung-Haing Cho[1,3,5–7]

[1]Laboratory of Toxicology, College of Veterinary Medicine, Seoul National University, Seoul, Korea; [2]School of Pharmacy, China Pharmaceutical University, Nanjing, China; [3]Department of Nanofusion Technology, Graduate School of Convergence Science and Technology, Seoul National University, Seoul, Korea; [4]Laboratory of Pathology, College of Veterinary Medicine, Seoul National University, Seoul, Korea; [5]Graduate Group of Tumor Biology, Seoul National University, Seoul, Korea; [6]Center for Food Safety and Toxicology, Seoul National University National Institute of Food and Drug Safety, Seoul, Korea; [7]Advanced Institute of Convergence Technology, Seoul National University, Suwon, Korea

Achievement of long-term survival of patients with lung cancer treated with conventional chemotherapy is still difficult for treatment of metastatic and advanced tumors. Despite recent progress in investigational therapies, survival rates are still disappointingly low and novel adjuvant and systemic therapies are urgently needed. A recently elucidated secretory pathway is attracting considerable interest as a promising anticancer target. The *cis*-Golgi matrix protein, GOLGA2/GM130, plays an important role in glycosylation and transport of protein in the secretory pathway. In this study, the effects of short hairpin RNA (shRNA) constructs targeting GOLGA2/GM130 (shGOLGA2) on autophagy and lung cancer growth were evaluated *in vitro* and *in vivo*. Downregulation of GOLGA2/GM130 led to induction of autophagy and inhibition of glycosylation in A549 cells and in the lungs of K-*ras*^{LA1} mice. Furthermore, downregulation of GOLGA2/GM130 decreased angiogenesis and cancer cell invasion *in vitro* and suppressed tumorigenesis in lung cancer mice model. The tumor specificity of sequence targeting GOLGA2/GM130 was also demonstrated. Taken together, these results suggest that induction of autophagy by shGOLGA2 may induce cell death rather than cell survival. Therefore, downregulation of GOLGA2/GM130 may be a potential therapeutic option for lung cancer.

Received 7 December 2011; accepted 29 May 2012; advance online publication 27 June 2012. doi:10.1038/mt.2012.125

INTRODUCTION

The Golgi apparatus is a central organelle in the secretory pathway of cells. It plays important roles in the posttranslational modification, sorting and transportation of all newly synthesized secretory proteins as well as transmembrane proteins from the endoplasmic reticulum (ER). The mechanisms of Golgi biogenesis and structural maintenance began to be revealed concomitant with the study of vesicular transport machinery in the late 1980s. It is known that the Golgi apparatus connects upstream (ER) or downstream (endosome, lysosome, and plasma membrane) compartments. This secretory pathway is being intensively studied in the development of novel targets for anticancer therapies.

GM130 (golgin A2; GOLGA2) is a *cis*-Golgi matrix protein that plays a major role in the stacking of Golgi cisternae and maintenance of Golgi structure.[1] It also participates in glycosylation and transport of proteins and lipids in the secretory pathway.[2] GOLGA2/GM130 knockdown inhibits the lateral cisternal fusion of Golgi stacks and disturbs the uniform distribution of Golgi enzymes affecting the glycosylation of secretory and membrane proteins,[3] and also results in a partial inhibition or delay of ER-to-Golgi transport.[4] In addition, glycosylation defects and temperature sensitivity of cell growth have been described in a mutant CHO cell line that lacks GOLGA2/GM130.[5]

Autophagy is a catabolic process involving the degradation of cytoplasmic proteins and organelles through lysosomal machinery. It is a major mechanism that promotes the survival of nutrient-starved cells. Autophagy also contributes to tumor suppression and defects of autophagy are associated with tumorigenesis.[6,7] Biochemical evidence indicates that autophagy is positively regulated by phosphatase and tensin homolog (PTEN) and negatively regulated by oncogenic class I phosphoinositol-3-kinase (PI3K) signaling.[8,9] Furthermore, the tumor suppressor activity of overexpressed mammalian autophagy gene, beclin 1 has been reported in several cancer cells and mice models.[7,10,11] Several studies have reported the role of autophagy-dependent death mechanism for tumor suppression.[6,12] Yet, how to exploit autophagy to improve therapeutic efficacy against cancer remains to be explored.

The importance of Golgi function associated with autophagy and poor prognosis of oncogenic lung diseases have prompted us to investigate the potential antitumor effects of the silencing of GOLGA2/GM130 production by the application of short

The first two authors equally contributed to this work.

Correspondence: *Myung-Haing Cho, Laboratory of Toxicology, College of Veterinary Medicine, Seoul National University, Gwanak-ro, Gwanak-gu, Seoul 151-742, South Korea. E-mail: mchotox@snu.ac.kr*

hairpin RNA (shRNA) constructs targeting GOLGA2/GM130 (shGOLGA2). Here, we report that delivery of shGOLGA2 suppresses lung tumorigenesis by inhibiting glycosylation as well as cell proliferation, which ultimately facilitates autophagic cell death. The results point the way to a possible alternate treatment of lung cancer.

RESULTS

Downregulation of GOLGA2/GM130 induces autophagy in A549 cells

To determine the silencing efficiency of four different shRNA constructs against GOLGA2/GM130, western blot was carried out in A549 cells. The results clearly showed that shGOLGA2 (no. 18 referred to shGOLGA2) significantly decreased GOLGA2/GM130 protein levels compared to scrambled and control as determined by western blot and densitometric analysis (**Figure 1b** and **Supplementary Figure S1a,b**). The distinct decrease of GOLGA2/GM130 mRNA expression was further confirmed by quantitative PCR (qPCR) (**Figure 1a**). Given that GOLGA2/GM130 is a *cis*-Golgi matrix protein that is crucial in stacking of Golgi cisternae and Golgi structure maintenance, it was appropriate to analyze the morphology of the Golgi apparatus when GOLGA2/GM130 was downregulated. Transmission electron microscopy (TEM) demonstrated swelling of Golgi cisternae and primary lysosomes (**Figure 1c**, arrow heads) and secondary lysosomes (autolysosomes; orange dotted circles in **Figure 1c**) in shGOLGA2-transfected cells. To determine whether downregulation of GOLGA2/GM130 was associated with autophagy, western blot and densitometric analyses of light chain 3 (LC3) was performed in shGOLGA2-treated cells. LC3 protein exists in two cellular forms; LC3-I and LC3-II. LC3-I, the cytoplasmic form, is processed by enzymatic cleavage into LC3-II, which is associated with the autophagosome membrane. Decreased GOLGA2/GM130 caused a significant increase in the ratio of LC3-II to LC3-I (**Figure 1d**). Therefore, an increase in the ratio of LC3-II to LC3-I coincides with autophagosome formation. Induction of autophagosomes in the cytoplasm of GOLGA2/GM130 downregulated cells was further confirmed by an immunofluorescence assay (**Figure 1e**). The formation of autophagosomes was clearly observed in GOLGA2/GM130 downregulated cells as well as in cells treated with brefeldin A (BFA). BFA disrupts the Golgi apparatus and secretory mechanism, and was used as a positive control because BFA induces autophagosome formation.[13,14]

Effect of shGOLGA2 on glycosylation and autophagy in A549 cells

To determine the effect of decreased GOLGA2/GM130 on protein glycosylation, the expression level of RL2 in GOLGA2/GM130 downregulated cells was assessed. The expression levels of RL2 were clearly decreased in a time-dependent manner, whereas an increase in the ratio of LC3-II to LC3-I was observed in GOLGA2/GM130 downregulated cells (**Figure 2a**). To further confirm GOLGA2/GM130-mediated regulation of protein glycosylation, cells were transfected with a GOLGA2/GM130 expression vector. Increased RL2 and a decrease in the ratio of LC3-II to LC3-I were clearly observed in GOLGA2/GM130-transfected cells (**Figure 2b**). Furthermore, the effect of decreased GOLGA2/GM130 on autophagy was detected by TEM. Stable downregulation of GOLGA2/GM130 in A549 cells resulted in formation of autophagosomes and accumulation of autophagic vesicles after 3 days, whereas after 4 and 7 days the accumulation of autophagic vesicles rather than autophagosomes was observed by TEM (**Figure 2c–e**). The collective observations clearly demonstrated that downregulation of GOLGA2/GM130 induced autophagy.

Effect of shGOLGA2 on angiogenesis, invasion, and proliferation of A549 cells

The effect of GOLGA2/GM130 on angiogenesis was assessed. qPCR and western blot analyses were carried out in A549 cells with stable GOLGA2/GM130 downregulation. The results showed decreased vascular endothelial growth factor (VEGF) and fibroblast growth factor-2 (FGF-2) expression levels in GOLGA2/GM130 downregulated cells (**Figure 3a,b**). Densitometric analysis confirmed the western blot results. In addition, the effect of GOLGA2/GM130 on cancer cell invasion was also determined. Large numbers of cells were found on the lower surface of control- and scramble-treated cells, whereas significant inhibition in the number of invading cells was observed in GOLGA2/GM130 downregulated cells as detected by light microscopy (**Figure 3c**). Significant reduction in fluorescence intensity was also measured in GOLGA2/GM130 downregulated cells as determined by fluorescence measurement (**Figure 3d**). In addition, the effect of GOLGA2/GM130 on cell proliferation was investigated. To determine whether or not downregulation of GOLGA2/GM130 affected cancer cell proliferation, xCELLigence was used to measure real-time cell proliferation. A significant decrease in proliferation was observed in GOLGA2/GM130 downregulated cells compared to control and scramble downregulated cells (**Figure 3e**). These results supported that the downregulation of GOLGA2/GM130 could suppress angiogenesis and invasion of lung cancer cells. Moreover, downregulation of GOLGA2/GM130 led to suppression of cancer cell proliferation.

Effect of shGOLGA2 in lung tumorigenesis of K-*ras*^{LA1} mice

The effect of shGOLGA2 was examined *in vivo* using K-*ras*^{LA1} mice. Pathological analysis performed in the lungs revealed that shGOLGA2 delivery suppressed lung tumor mass in the lungs of 10-week-old mice (**Figure 4a**). The number and volume of lung tumors also were significantly decreased by GPT-SPE/shGOLGA2 delivery (**Figure 4b,c**). The suppression of lung tumor formation was further confirmed by histological examination (**Figure 4d**). The nodules that developed in the lungs of control (Con) and scramble-delivered (shScr) groups were, in general, alveolar/bronchial adenocarcinoma and moderate adenoma, whereas only mild adenomas were observed in the shGOLGA2-delivered group (shGOLGA2), in which progression to adenocarcinoma was inhibited (**Table 1**). These findings clearly showed that aerosol delivery of GPT-SPE/shGOLGA2 suppressed tumor progression to lung adenocarcinoma.

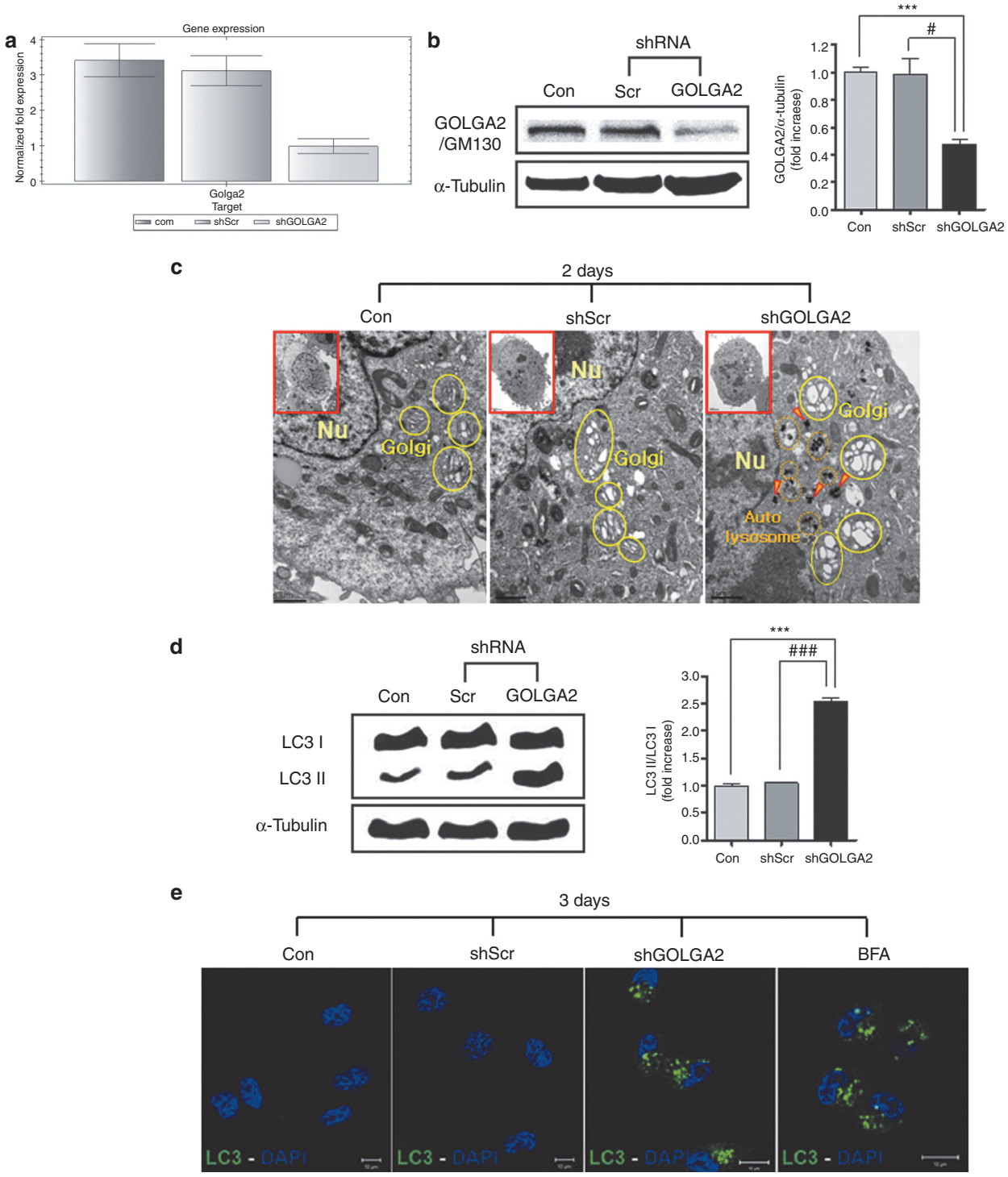

Figure 1 Downregulation of GOLGA2/GM130 by shGOLGA2 induces autophagy in A549 cells. (**a**) qPCR analysis of GOLGA2/GM130. Stably downregulated cells were cultured for 24 hours and then total RNA from cultured cells was isolated and cDNA synthesized, then subjected to qPCR. Values represent mean ± SEM ($n = 4$). (**b**,**d**) Western blot analysis of GOLGA2/GM130 and LC3. Cell lysates were subjected to western blot analysis. Blots were probed with antibody of GM130 (mouse monoclonal IgG2a; Santa Cruz Biotechnology, Santa Cruz, CA) or MAP1LC3 (Purified Mouse Monoclonal Antibody; ABGENT, San Diego, CA). The right panel shows the results of densitometric analysis of bands-of-interest. Values are the means ± SEM ($n = 3$). $^{\#}P < 0.05$ was considered significant and $^{***}P < 0.001$ or $^{\#\#\#}P < 0.001$ highly significant compared with corresponding control values. (**c**) Representative result of TEM analysis; A549 cells that stably downregulated GOLGA2/GM130 (shGOLGA2), scramble (shScr), or control (Con) were cultured for 2 days and imaged by TEM. Arrow heads and orange dotted circles indicate the primary and secondary lysosomes, respectively. The bar represents 1 µm. (**e**) Immunofluorescence of LC3 in A549 cells with downregulated GOLGA2 (shGOLGA2), scramble (shScr), or control (Con). Stably downregulated cells were incubated for 3 days, followed by fixing and immunostaining for LC3 (green *via* Alexa Fluor 488) and nuclei (blue *via* DAPI). BFA (1 µg/ml) as the positive control was pre-treated for 24 hours. The bar represents 10 µm. BFA, brefeldin A; DAPI, 4′,6-diamidino-2-phenylindole; Golgi, golgi apparatus; Nu, nucleus; qPCR, quantitative PCR; shRNA, short hairpin RNA; TEM, transmission electron microscopy.

Downregulation of GOLGA2/GM130 induces autophagy in the lungs of K-*ras*^{LA1} mice

To examine whether repeated aerosol delivery of GPT-SPE/shGOLGA2 can induce autophagy in the lungs of K-*ras*^{LA1} mice, qPCR, western blot, and immunohistochemistry (IHC) analyses were performed to quantify mRNA and protein expression levels. Repeated aerosol delivery of GPT-SPE/shGOLGA2 significantly decreased mRNA level of GOLGA2/GM130 and protein levels of GOLGA2/GM130 and RL2, whereas an increase in the ratio of LC3-II to LC3-I was observed (**Figures 5a–c**). IHC analysis demonstrated that aerosol-delivered GPT-SPE/shGOLGA2 increased the expression of LC3 in the lungs of K-*ras*^{LA1} mice (**Figure 5d**). Determining the relative intensity of staining for LC3 further supported this finding (lower panel of **Figure 5d**). The effect of shGOLGA2 on normal and tumor tissue in the lungs of K-*ras*^{LA1} mice was examined. TEM results showed that shGOLGA2

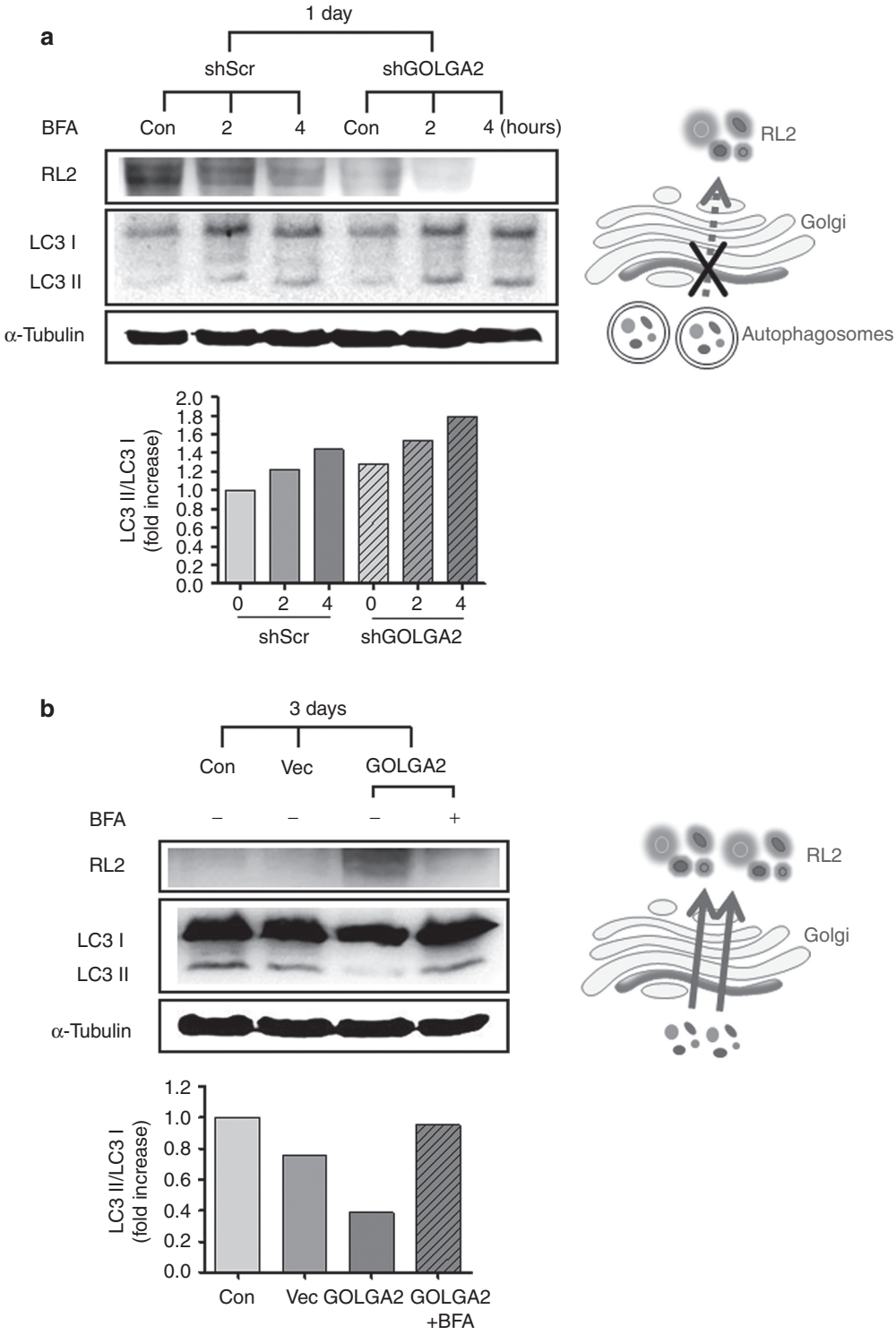

delivery caused formation of autophagosome at tumor tissue as demonstrated (**Figure 5e**). The sequence targeting GOLGA2/GM130 was tumor-specific because the aforementioned effects were not observed in normal lung cells (**Supplementary Figure S2**) and normal lung tissue (type II alveolar cells; **Figure 5e**). Together, these results clearly demonstrated that downregulation of GOLGA2/GM130 induced tumor-specific autophagy in the lungs of K-*ras*^{LA1} mice.

Downregulation of GOLGA2/GM130 suppresses angiogenesis and cell proliferation in the lung of K-*ras*^{LA1} mice

Whether downregulation of GOLGA2/GM130 would alter angiogenesis in the lungs of K-*ras*^{LA1} mice was assessed. Western blot and IHC analyses were carried out in the lungs of K-*ras*^{LA1} mice. The levels of both VEGF and FGF-2 were significantly decreased in the lungs of shGOLGA2-delivered mice compared to the lungs of scramble (shScr)-delivered mice as well as control mice (**Figure 6a,b**). Moreover, decreased level of cluster of differentiation 31 (CD31), a endothelial cell marker, was further confirmed in shGOLGA2-delivered mice (**Figure 6c,d**). The effect of shGOLGA2 on cell proliferation was also investigated. shGOLGA2-delivered mice clearly decreased the cell proliferation marker proliferating cell nuclear antigen (PCNA), as detected by western blot and IHC determination of the relative staining intensity (**Figure 6e,f**). The results clearly demonstrated that downregulation of GOLGA2/GM130 suppresses angiogenesis and cell proliferation in the lungs of K-*ras*^{LA1} mice.

DISCUSSION

In cancer therapy, tumor cell death is an important event in the elimination of abnormal malignant cells. Anticancer therapies for

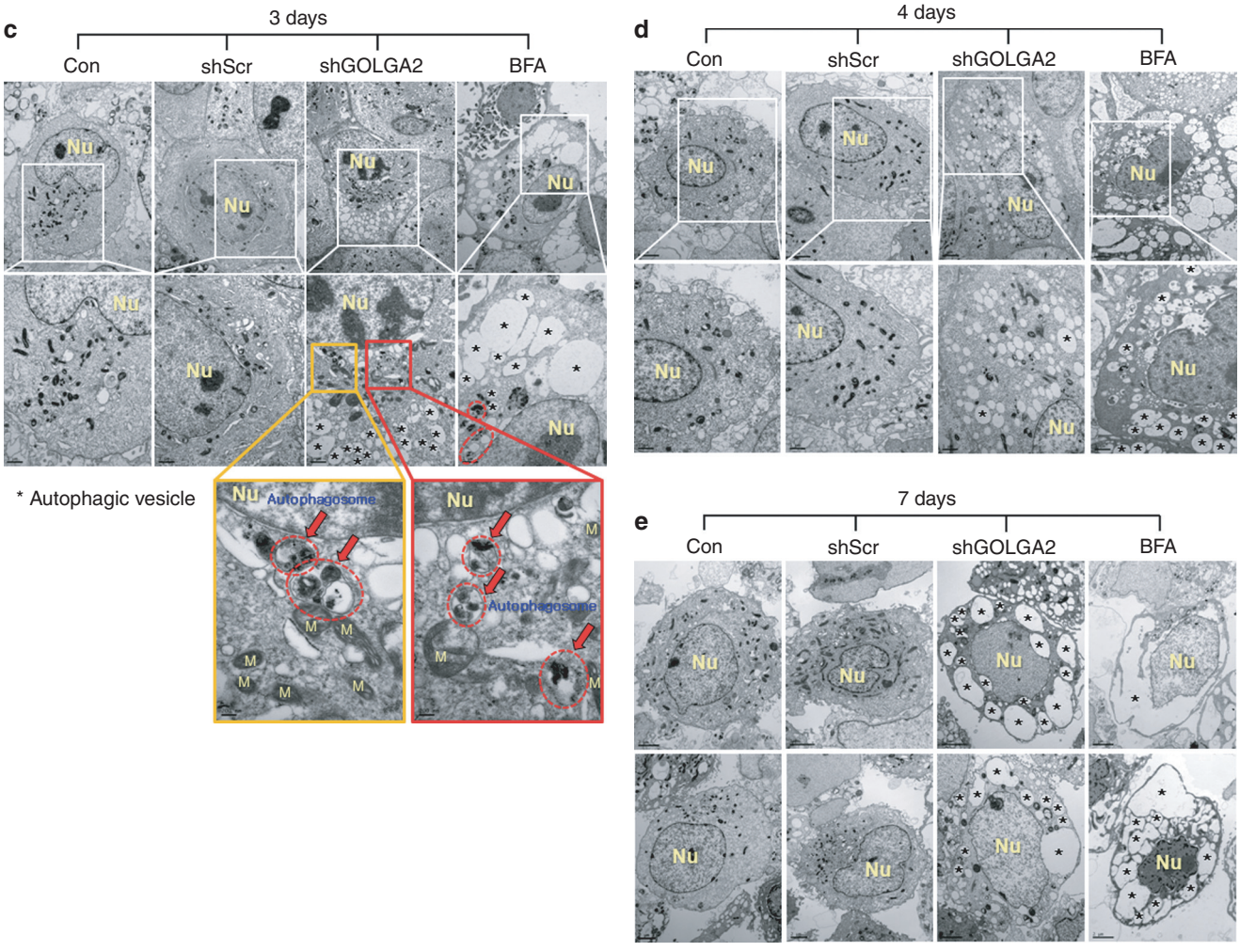

Figure 2 Downregulation of GOLGA2/GM130 suppresses glycosylation of protein and induces autophagy in A549 cells. (**a**,**b**) Western blot analysis of RL2 and LC3. Stably downregulated cells were pre-treated with BFA (1 µg/ml) for 2 or 4 hours and then harvested for western blot analysis (RL2, anti-O-Linked N-Acetylglucosamine monoclonal antibody; Thermo Fisher Scientific, San Jose, CA). A549 cells were transiently transfected with GOLGA2/GM130 expression vector or control vector (Vec), and GOLGA2/GM130 overexpressed cells were pre-treated with BFA (1 µg/ml) for 4 hours. The right panel depicts a schematic model showing the proposed mechanism of the effect of GOLGA2/GM130 on the secretory pathway. (**c**–**e**) TEM analysis of stably downregulated cells. Cells were incubated for 3, 4 or 7 days with fresh media that were changed every day, fixed, and analyzed via TEM. BFA-treated cells were used as an autophagy positive control. Arrows and red dotted circles indicate autophagosomes. The bars represents 2, 1, and 0.2 µm. Asterisk (*) indicates autophagic vesicle (AV). BFA, brefeldin A; M, mitochondria; Nu, nucleus; TEM, transmission electron microscopy.

elimination of malignant cells often depend on classical caspase-dependent apoptosis.[15–17] However, recent evidence indicates that several alternative cell death pathways, including caspase-independent programmed cell death, necrosis-like programmed cell death, mitotic or autophagic cell death are present.[12,18–21] In the context of cancer therapy, novel pathways involving the ER, Golgi apparatus, and lysosomes are being recognized as potential targets for therapeutic interventions.[21,22] Recent evidence supports the involvement of the secretory pathway can initiate and propagate cell death signaling.[23] ER and Golgi apparatus can activate

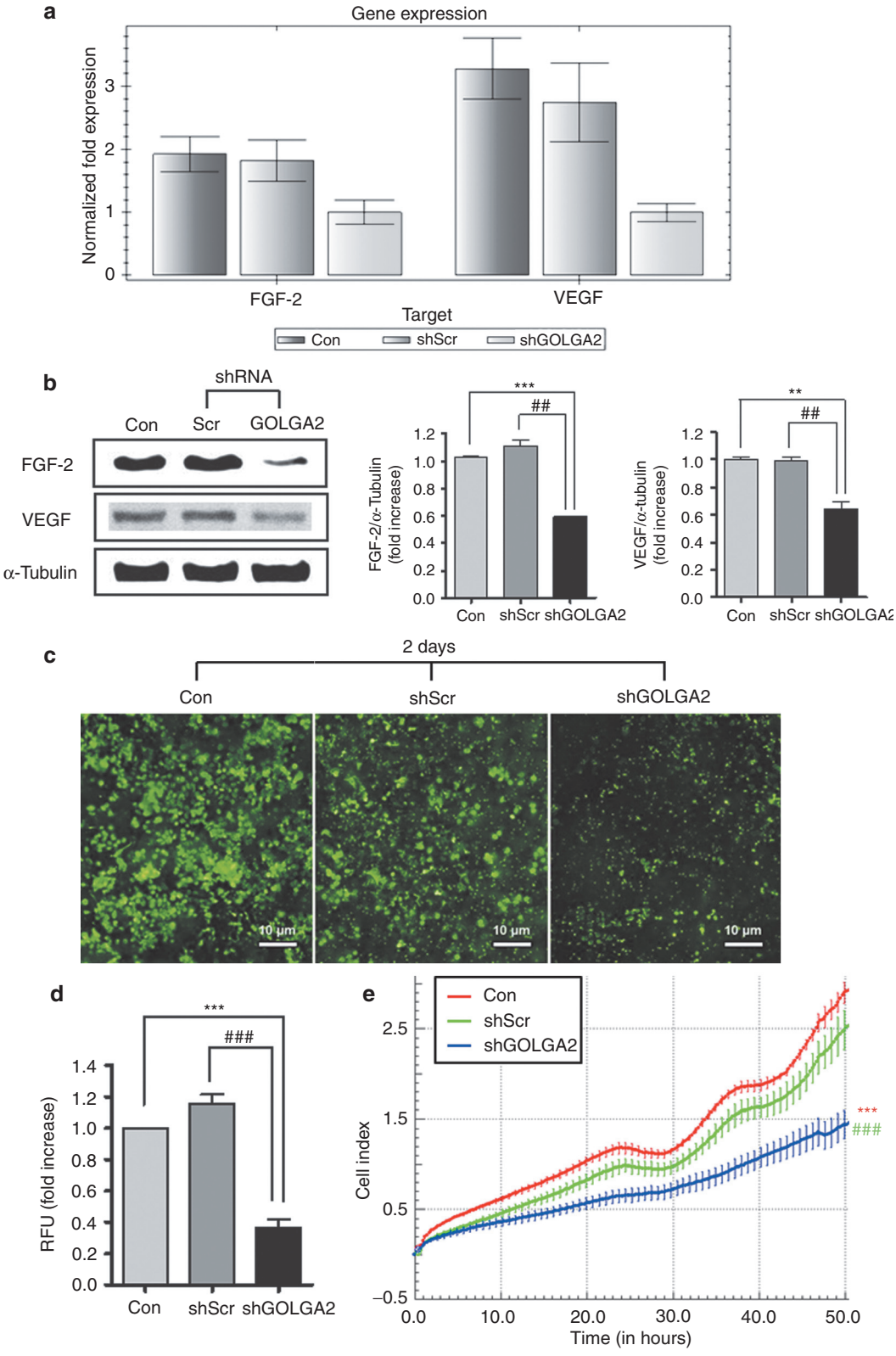

both pro-survival mechanisms and cell suicide programs.[23,24] Therefore, the control of trafficking between ER and Golgi may provide therapeutic opportunities to treat the cancer. In this study, we attempted to alter the balance of protein trafficking between ER and Golgi using shRNA-GOLGA2/GM130 (shGOLGA2) as an anticancer molecule. Swelling of Golgi cisternae and formation of autolysosomes were evident in GOLGA2/GM130 downregulated cells (**Figure 1c**), suggesting that inhibition of protein trafficking between ER and Golgi may lead to autophagy. Cisternal swelling of Golgi and the formation of autolysosomes (fusion of autophagosomes and primary lysosomes) have been detected during autophagy.[25] Furthermore, our data is consistent with a previous report indicating that inhibition of protein glycosylation by BFA, which blocks transport of proteins from the ER to the Golgi, can induce autophagosome formation (**Figure 2**).[14] It has been shown that small interfering RNA against GOLGA2/GM130 results in accumulation of vesicular membranes and an inhibition of ER-to-Golgi transport.[26]

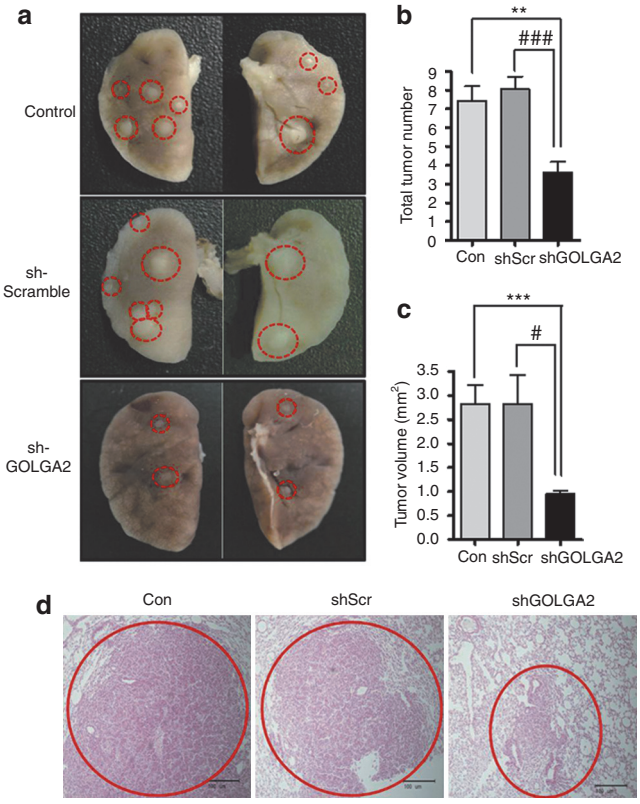

Figure 4 Downregulation of GOLGA2/GM130 suppresses tumorigenesis in the lungs of K-ras^{LA1} mice. (**a**) Tumor pathology of the lungs in K-*ras*^{LA1} mice. Pathological examination of lungs of K-*ras*^{LA1} mice exposed to aerosols containing GPT-SPE/shGOLGA2 twice a week for totally 4 weeks. Red dotted circles indicate the tumor mass in the lungs of K-*ras*^{LA1} mice. (**b**,**c**) Total tumor number and tumor volume in the lungs of K-*ras*^{LA1} mice; the mean tumor diameter of at least 1.0 mm was counted in the lungs of 10-week-old K-*ras*^{LA1} mice. Values are the means ± SEM ($n = 6$). $^{**}P < 0.01$, $^{***}P < 0.001$, $^{\#}P < 0.05$ or $^{\#\#\#}P < 0.001$ considered significant compared with corresponding control values. (**d**) Histological examination of lungs in K-*ras*^{LA1} mice. Red circles indicate the adenocarcinoma or adenoma in the lungs of K-*ras*^{LA1} mice. The bar represents 100 µm.

The relationship between different types of altered glycosylation and prognosis of tumor-bearing animals has attracted much attention in this changes.[27] However, the exact mechanism by which changes in glycosylation affect tumor behavior has not been elucidated. To address this issue, we investigated the changes in protein glycosylation using shGOLGA2 and showed that inhibition of glycosylation may induce autophagy leading to the suppression of cancer cell growth both *in vitro* and *in vivo*. Similarly, tunicamycin, which is a specific inhibitor of N-glycosylation, induces autophagy.[28] Our results suggest that unglycosylated proteins by shGOLGA2 may lead to induction of autophagy.

Autophagy constitutes a stress adaptation that avoids cell death during nutrient starvation and suppresses apoptosis.[29] In other cellular settings, autophagy constitutes an alternative cell death pathway.[6,12] Autophagy and apoptosis may be triggered by common upstream signals, sometimes resulting in combined autophagy and apoptosis, whereas, in other instances, cells switch between the two responses in a mutually exclusive manner.[22,30] In a previous study, we showed that A549 cells having stably elevated *BECN1* expression significantly increased the ratio of LC3-II to LC3-I, whereas decreased levels of apoptosis-related proteins such as Bax and cleaved PARP were observed.[31] In the current study, we also examined the effect of shGOLGA2 on apoptosis and autophagy. Induction of LC3-II and reduction of Bax protein levels were observed in shGOLGA2 downregulated cells as detected by western blotting analysis (data not shown). Thus, our results indicate that suppressed cell growth *in vitro* and *in vivo* may cause autophagy.

Table 1 Histopathology in the lungs of K-*ras*^{LA1} mice

Group	Number of mice	Adenocarcinoma incidence	Adenoma	
			++	+
Con	6	2	3	1
shScr	6	1	3	2
shGOLGA2	6	0	0	6

++: adenoma grade was moderate; +: adenoma grade was mild.

Figure 3 Downregulation of GOLGA2/GM130 suppresses angiogenesis and invasion in A549 cells. (**a**) qPCR analysis of angiogenesis. Total RNA from cultured cells for 72 hours was isolated and cDNA synthesized, and then subjected to qPCR. Values represent mean ± SEM ($n = 4$). (**b**) Western blot analysis of angiogenesis. Cell lysates were subjected to western blot analysis. Blots were probed with antibody of FGF-2 (rabbit polyclonal IgG; Santa Cruz Biotechnology) or VEGF (mouse monoclonal IgG2a; Santa Cruz Biotechnology). The right panels summarize the results of densitometry analysis of the bands-of-interest. Values represent mean ± SEM ($n = 3$). $^{**}P < 0.01$, $^{***}P < 0.001$ or $^{\#\#}P < 0.01$, $^{\#\#\#}P < 0.001$ highly significant compared with corresponding control values. (**c**) Invasion assay in A549 cells with downregulated GOLGA2/GM130, scramble or control. Stably downregulated cells were added to the invasion chamber and cultured for 48 hours. After growth, invading cells were stained with CyQuant GR dye (green) and viewed by light microscopy. The bar represents 10 µm. (**d**) For measuring the relative intensity of invasion, cells stained with CyQuant GR dye and read by multiple plate reader. Values are the mean ± SEM ($n = 3$). $^{***}P < 0.001$ or $^{\#\#\#}P < 0.001$ highly significant compared with corresponding control values. (**e**) Real-time cell proliferation assay; stably downregulated cells were measured using an xCELLigence RTCA DP system for 50 hours ($n = 4$). Values are the means ± SEM. $^{***}P < 0.001$ versus Con (control, red line), $^{\#\#\#}P < 0.001$ versus shScr (scramble, green line). FGF, fibroblast growth factor; qPCR, quantitative PCR; RFU, relative fluorescence unit; shRNA, short hairpin RNA; VEGF, vascular endothelial growth factor.

Recent reports support the view that autophagic cell death inhibits angiogenesis. The angiogenesis inhibitor, endostatin, induces autophagic cell death in human endothelial cell.[32] In addition, the tumor suppressor gene, PTEN, induces autophagy and inhibits angiogenesis in a nude mouse orthotopic brain tumor model.[33] Thus, the autophagy in tumor angiogenesis might play an important role for inhibiting tumor progression and increasing effectiveness of anticancer therapy. The present *in vitro* and *in vivo* results clearly demonstrated that the downregulation of GOLGA2/GM130 decreased VEGF and FGF-2 protein levels as well as cancer cell invasion, which can lead to inhibition of angiogenesis (**Figures 3a–d** and **6a,b**). Moreover, we also showed suppression of endothelial cell marker, CD31, and cancer cell proliferative marker, PCNA, in the lungs of shGOLGA2-delivered K-*ras*^{LA1} mice (**Figure 6c–f**). Therefore, in this study, we report that suppression of angiogenesis can inhibit tumor growth in GOLGA2/GM130 downregulated A549 cells and the lungs of shGOLGA2-delivered K-*ras*^{LA1} mice.

Interestingly, our results indicated that the sequence targeting GOLGA2/GM130 can perform its proper silencing effect in tumors that led to the inhibition of tumorigenesis because it did not show a silencing effect in normal lung cells (**Supplementary Figure S2**) and normal tissue in the lungs (type II alveolar cells; **Figure 5e**). Also, immunohistochemical results indicate the induction of LC3

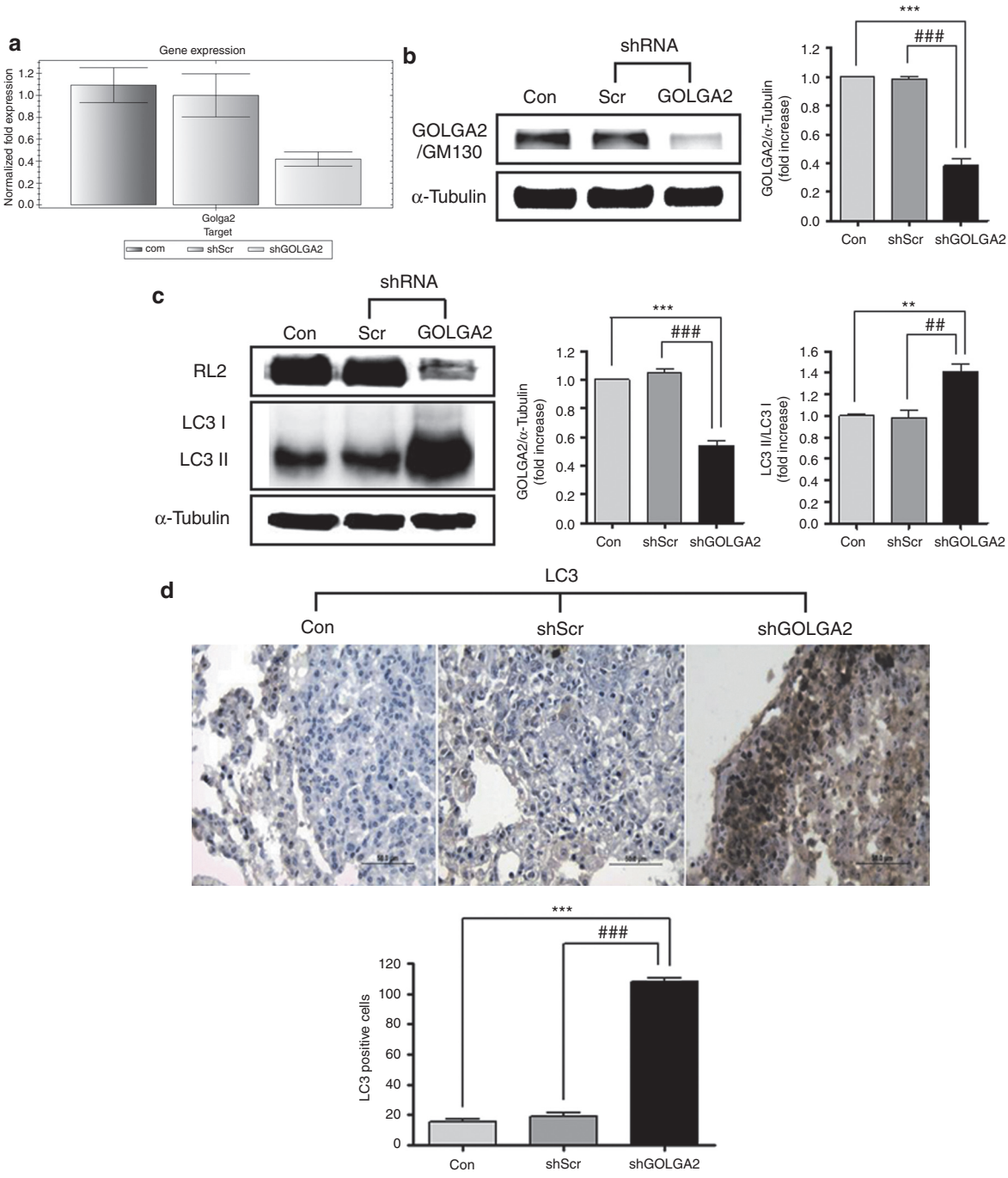

and reduction of VEGF, CD31, and PCNA in tumors (**Figures 5d** and **6b,d,f**). This finding is a significant event for tumor-specific therapeutic strategy. However, future experiments are necessary to clarify the proposed mechanism of the effect of GOLGA2/GM130 on tumor cells. These studies are currently under way.

Taken together, the present results indicate that the induction of autophagy by the expression of shGOLGA2 may induce cell death rather than cell survival. Thus, the downregulation of GOLGA2/GM130 may offer new therapeutic opportunities to treat lung cancer.

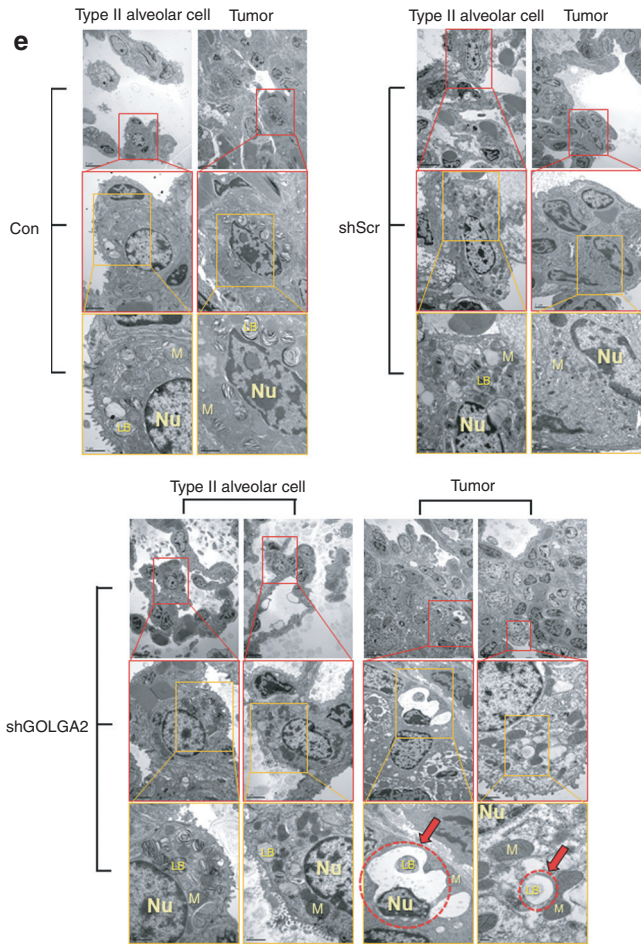

Figure 5 Downregulation of GOLGA2/GM130 induces autophagy in the lungs of K-ras^{LA1} mice. (**a**) qPCR analysis of GOLGA2/GM130. Total RNA from lung tissue was isolated and cDNA synthesized, and then subjected to qPCR. Values represent mean ± SEM ($n = 4$). (**b**,**c**) Western blot analysis of GOLGA2/GM130, RL2, and LC3. Lung tissue homogenates were subjected to western blot analysis. Blots were probed with antibodies as indicated. The right panel shows the results of densitometric analysis of the bands-of-interest. Values are the mean ± SEM ($n = 3$). $^{**}P < 0.01$, $^{***}P < 0.001$ or $^{\#\#\#}P < 0.001$, $^{\#\#}P < 0.001$highly significant compared with corresponding control values. (**d**) Immunohistochemistry analysis of LC3 in the lung. Dark brown color indicates LC3 expression. The bar represents 50 µm. The lower panel displays the results of the comparison of LC3 labeling index. LC3 positive staining was determines the percentage of diaminobenzidine-positive cells per 100 cells at ×400 magnification. Values are the mean ± SEM ($n = 4$). $^{***}P < 0.001$ or $^{\#\#\#}P < 0.001$ highly significant compared with corresponding control values. (**e**) TEM analysis of the lungs in K-ras^{LA1} mice. Lung tissue was fixed and analyzed. Arrow and red dotted circles indicate the autophagosome. The bar represents 5 (top), 2 (middle), 1 (bottom) µm. LB, lamellar body; M, mitochondria; Nu, nucleus; qPCR, quantitative PCR; shRNA, short hairpin RNA; TEM, transmission electron microscopy.

MATERIALS AND METHODS

Cell culture and generation of GOLGA2/GM130 downregulated stable cell line. A549 cell line was obtained from American Type Culture Collection (Rockville, MD) and was transfected with four kinds of shRNAs targeting GOLGA2/GM130 (**Supplementary Figure S1a**) (OriGene Technologies, Rockville, MD). The short interfering RNA sequence 5′ -C AGCTTTCTGGAGAGACAGACACCATTGG-3′ (no. Fl350818) refers to shGOLGA2. For transfections, A549 cells (1×10^6) were grown in a T25 flask and were transfected with each plasmid using TransIT^R-LT1 reagent (Mirus Bio, Madison, WI). After transfection, cells were selected with medium containing 1 µg/ml of puromycin (InvivoGen, San Diego, CA). A549 and all selected stable cell lines were grown in RPMI-1640 medium supplemented with 10% fetal bovine serum and 1% penicillin/streptomycin (GibcoBRL, Grand Island, NY).

In vivo aerosol delivery of GPT-SPE/shGOLGA2. All animals used in this study were maintained under animal protocols of Seoul National University guidelines and the study was approved by the Animal Care and Use Committee at Seoul National University (SNU-110626-1; Seoul, Korea). Breeding K-*ras*^{LA1} mice, which are an accepted model of human non-small cell lung cancer, were obtained from Human Cancer Consortium-National Cancer Institute (Frederick, MD) and kept in the laboratory animal facility with temperature and relative humidity maintained at 23 ± 2 °C and 50 ± 20%, respectively, under a 12-hour light/dark cycle. To ascertain the effects of shGOLGA2 against lung cancer development, the K-*ras*^{LA1} mice were divided into three groups. Experiments were performed on 6-week-old male K-*ras*^{LA1} mice ($n = 6$ per group). The control group was untreated. The other two groups were exposed to an aerosol containing GPT-SPE/shGOLGA2 or GPT-SPE/scramble. GPT-SPE is a biocompatible aerosol gene delivery carrier that was prepared as previously described.[34] The K-*ras*^{LA1} mice exposed to shGOLGA2 were placed in a nose-only exposure chamber and exposed to aerosol containing the GPT-SPE/shGOLGA2 solution (50 ml) containing 1 mg of shGOLGA2 plasmid twice a week for 4 weeks. At the end of study, the mice were killed and the lungs were carefully collected. During necropsy, the neoplastic lesions of lung surfaces were carefully counted under a microscope and the lesion diameters were measured with the aid of a digital caliper.[35] The volume of tumors with a diameter exceeding 1.0 mm was calculated based on formulae described elsewhere.[36] Simultaneously, the lungs were fixed in 10% neutral-buffered formalin for histopathological examination and IHC. After experiments, remaining lungs were stored at −70 °C for further analysis.

Histopathology and IHC. The lung tissue were collected and fixed in 10% neutral-buffered formalin. After paraffin embedding, tissue sections were cut at a thickness of 3 µm and transferred to a Plus slide (Fisher Scientific, Pittsburgh, PA). For histological analysis, the tissue sections were routinely processed and stained with hematoxylin and eosin. For IHC, tissue sections were deparaffinized in xylene and rehydrated through in serial alcohol gradient 100–50% each for 2 minutes, then washed and immersed in 3% hydrogen peroxide (AppliChem, Darmstadt, Germany) for 20 minutes to quench endogenous peroxidase activity. After washing in TTBS (Tris-Buffered Saline + Tween 20) solution, tissue slides were incubated with 3% bovine serum albumin (BSA) in TTBS for 1 hour at room temperature for the blocking of unspecific binding sites. Appropriate primary antibodies (dilution of 1:100 in 3% BSA) were applied on tissue slides at 4 °C overnight. After washing in TTBS, secondary horseradish peroxide-conjugated antibodies (Invitrogen, Carlsbad, CA; diluted 1:50 in 3% BSA) were applied to the tissue slides for 3 hours at room temperature. After careful washing, tissue sections were reacted with 3,3′ -diaminobenzidinetetrahydrochloride substrate (DAB; Biosesang, Sungnam, Korea) and observed using a light

microscope (Carl Zeiss, Thornwood, NY) for the appropriate reaction and washed with distilled water. After washing in distilled water, tissue sections were counterstained with Mayer's hematoxylin (DAKO, Carpinteria, CA) and washed with xylene. Tissue slides were mounted using cover slips and Permount (Fisher Scientific), and the slides were examined using the aforementioned light microscope. Staining intensities of microtubule-associated protein LC3, VEGF, CD31, and PCNA were analyzed using In Studio version 3.01 (Pixera, San Jose, CA) by counting the number of positive cells in randomly selected fields viewed with appropriate magnification of the objective lens.

TEM. A549 cells and lung tissue were fixed with a solution of 2.5% glutaraldehyde with 1% osmium tetroxide (OsO_4) buffer for 2 hours at 4 °C and dehydrated with ethanol at 4 °C. Then, cells and tissues were infiltrated in a 1:1 mixture of propylene oxide and Epon, and finally embedded in Epon by polymerization at 70 °C for 24 hours. Ultrathin sections (40–70 nm) were cut and mounted on pioloform-coated copper grids. Sections were stained with lead citrate and uranyl acetate and viewed with a JEM 1010 transmission electron microscope (JEOL, Tokyo, Japan).

DAPI and immunostaining. Cells (1×10^4) were seeded in two-well chamber slides and incubated for 3 days. Slides were washed with phosphate-buffered saline and fixed in 4% paraformaldehyde for 10 minutes at 37 °C. Cells were washed and fixed again with methanol:acetone (1:1, vol/vol). After being blocked with 3% BSA in TTBS for 1 hour, cells were incubated in a 1:500 dilution of primary antibody overnight at 4 °C, washed and incubated in a 1:500 dilution of Alexa Fluor 488-conjugated secondary antibody for 2 hours at room temperature. After washing, coverslips

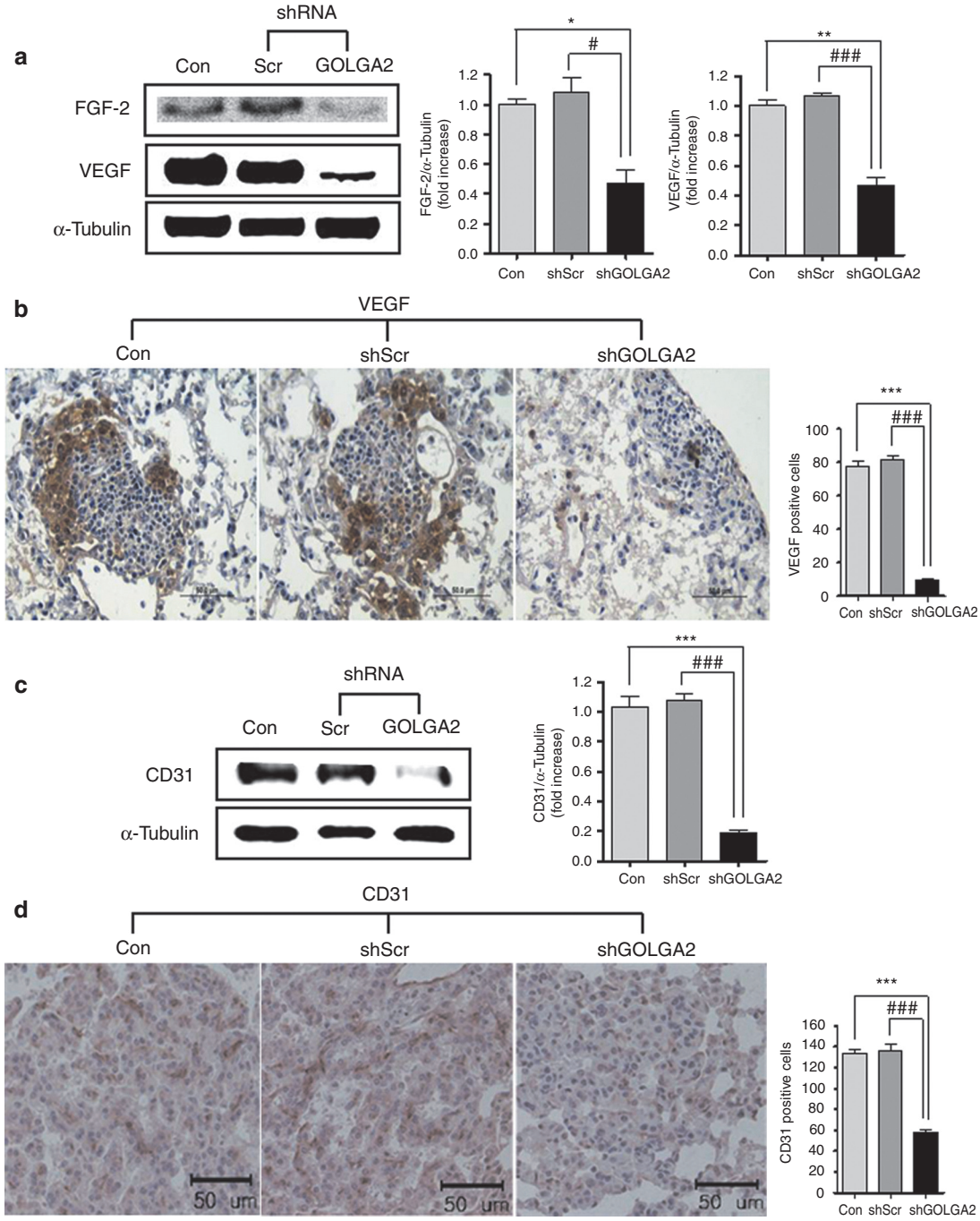

were mounted using FLUOROSHIELD^{T} mounting medium with DAPI (ImmunoBioScience, Mukilteo, WA). The slides were visualized using a fluorescent microscope (Carl Zeiss).

Western blot analysis. After measuring the protein concentration of the lysates using a Bradford Protein Assay Kit (Bio-Rad, Hercules, CA), equal amounts (25 µg) of protein were separated by 10–15% sodium dodecyl sulfate-polyacrylamide gel electrophoresis (SDS-PAGE) and transferred to nitrocellulose membranes. Membranes were blocked with TTBS containing 5% skim milk for 1 hour at room temperature and immunoblotting was performed by incubation overnight at 4 °C with the corresponding primary antibodies in 5% skim milk and then with secondary antibodies conjugated to horseradish peroxide for 1 hour at room temperature. After washing, the bands-of-interest were visualized using a model LAS-3000 luminescent image analyzer (Fujifilm, Tokyo, Japan).

Real-time qPCR. Total RNA was isolated using QuickGene RNA cultured cell kit (Fujifilm's Life Science System, Tokyo, Japan), and then subjected to SuPrimeScript RT Premix (GeNet Bio, Nonsan, Korea) and reverse transcription reaction was performed at the following cycling conditions: 25 °C for 10 minutes, 37 °C for 30 minutes, 85 °C for 5 minutes. Real-time qPCR was performed with CFX96^{T} Real-Time System (Bio-Rad). Each cDNA was amplified with specific primer and Prime Q-Mastermix (GeNet Bio) at the following cycling conditions: initial denaturation at 94 °C for 10 minutes; denaturing at 94 °C for 30 seconds, annealing at 53 °C for 30 seconds, and extension at 72 °C for 45 seconds, 40 cycles; final extension at 72 °C for 5 minutes. The sequences of primers used for qPCR were: human GOLGA2/GM130, forward (5′ -AACGACCGCACTACCATC-3′) and reverse (5′ -GGTGATCTCCATGTTCTCATTAG-3′); human FGF-2, forward (5′ -TGGTTAGAAACAACTGAAAGCATA-3′) and reverse (5′ -TGAACTCCTGGGCTCAAG-3′); human VEGF, forward (5′ -CGAGTACATCTTCAAGCCATC-3′) and reverse (5′ -GTGAGGTTTGATCCGCATAA-3′); human α-tubulin, forward (5′ -ACCTCTCCTCTTCGTCTC-3′) and reverse (5′ -GTGTTCCAGGCAGTAGAG-3′); mouse GOLGA2/GM130, forward (5′ -CAGGCAGACAGGTATAACAAG-3′) and reverse (5′ -CGGAGTTTCTCTTCCAGTTC-3′); mouse α-tubulin, forward (5′ -CACACATTGCCACATACAAAT-3′) and reverse (5′ -AGGAAGAAGGAGAGGAATACTAA-3′). Products were analyzed by Bio-Rad CFX Manager Version 2.1 Software (Bio-Rad).

Cell invasion assay. Cancer cell invasion assay was performed in a CytoSelect 24-Well Cell Invasion Assay kit (Cell Biolabs, San Diego, CA). The cells (2×10^5) were added to the invasion chamber and cultured for 48 hours. After growing, noninvasive cells were removed from upper surface of the membrane with a cotton-tipped swab. The invasive cells on the bottom of the invasion membrane were stained with CyQuant GR dye solution and viewed under a BX51 light microscope (Olympus, Tokyo, Japan) attached with a fluorescence lamp power supply (Olympus). To measure the relative intensity of invasion, cells stained with CyQuant GR dye were read by Perkin Elmer Victor3 Multiple Plate Reader (Wallac, Turku, Finland) at 490 nm.

Real-time cell proliferation assay. Real-time cell proliferation was measured using an xCELLigence RTCA DP system (Roche Applied Science, Indianapolis, IN) which monitors cellular events in real-time without the incorporation of labels. Briefly, 2.5×10^3 cells were placed into well of an E-plate 16 and incubated for 50 hours. This system measures electrical impedance across interdigitated microelectrodes integrated on the bottom

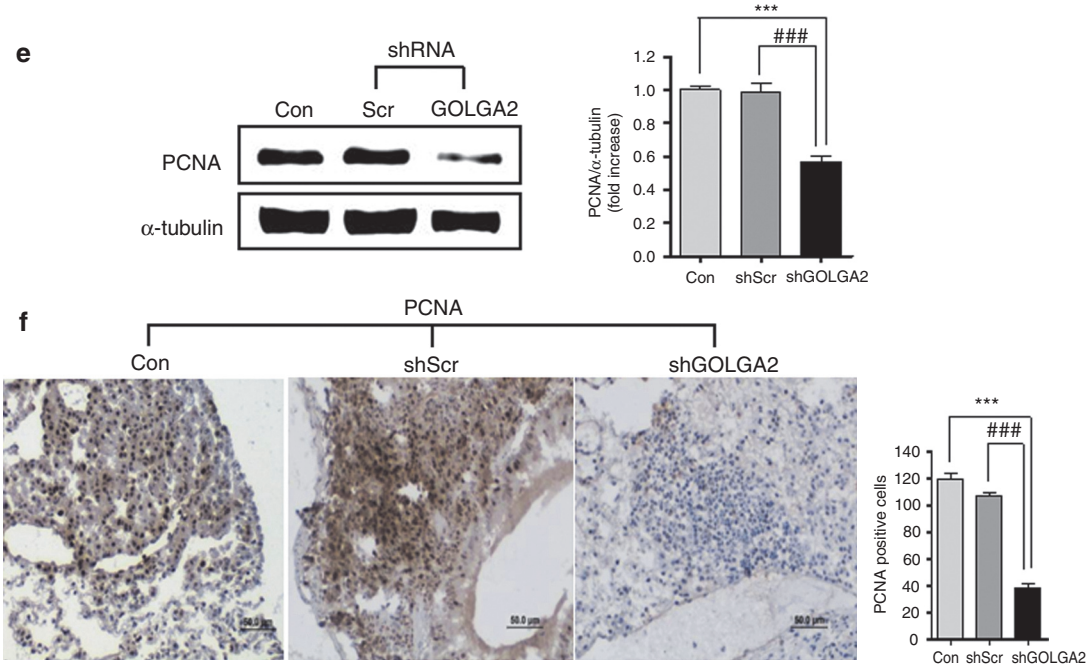

Figure 6 Downregulation of GOLGA2/GM130 suppresses angiogenesis and proliferation in the lungs of K-ras^{LA1} mice. (**a**,**c**,**e**) Western blot analyses of FGF-2, VEGF, CD31 (purified anti-mouse CD31; BD Pharmingen, San Jose, CA) and PCNA (mouse monoclonal IgG2a; Santa Cruz Biotechnology). Lung tissue homogenates were subjected to western blot analysis. Blots were probed with antibodies as indicated. The right panel shows the results of densitometric analysis of the bands-of-interest. Values are the mean ± SEM ($n = 3$). $^{*}P < 0.05$ or $^{\#}P < 0.05$ was considered significant and $^{**}P < 0.01$, $^{***}P < 0.001$ or $^{\#\#}P < 0.01$, $^{\#\#\#}P < 0.001$ highly significant compared with corresponding control values. (**b**,**d**,**f**) Immunohistochemistry analyses of VEGF, CD31, and PCNA in the lung. Dark brown color indicates the expression. The bar represents 50 µm. The right panel shows results of the comparison of LC3, CD31 or PCNA labeling. LC3, CD31 or PCNA positive staining determines the percentage of diaminobenzidine-positive cells per 100 cells at ×400 magnification. Values are the mean ± SEM ($n = 4$). $^{***}P < 0.001$ or $^{\#\#\#}P < 0.001$ highly significant compared with corresponding control values. FGF, fibroblast growth factor; PCNA, proliferating cell nuclear antigen; shRNA, short hairpin RNA; VEGF, vascular endothelial growth factor.

of tissue culture E-Plates. The impedance measurement provides quantitative information about the biological status of the cells, including cell number, viability, and morphology.

Statistical analysis. Data are expressed as mean ± SEM. Student's *t*-test was used for comparison between two groups. All statistical analyses were performed using GraphPad Software version 4.02 (GraphPad Software, San Diego, CA). $^{*}P < 0.05$ was considered significant and $^{**}P < 0.01$ and $^{***}P < 0.001$ were highly significant compared with the corresponding control values. Quantification of western blot analysis was conducted using the Multi Gauge version 3.0 program (Fujifilm).

ACKNOWLEDGMENTS

This work was supported by the National Research Foundation (NRF-2012-0000102) of the Ministry of Education, Science and Technology (MEST) in Korea. M.-H. Cho was also partially supported by the Research Institute for Veterinary Science, Seoul National University. The authors declared no conflict of interest.

SUPPLEMENTARY MATERIAL

Figure S1. Sequence against GOLGA2 and its impact on GOLGA2/GM130 expression levels of A549 cells (cancer cells).

Figure S2. Sequence against GOLGA2 and its impact on GOLGA2/GM130 expression levels of 16HBE14o- cells (normal cells).

REFERENCES

1. Nakamura, N, Rabouille, C, Watson, R, Nilsson, T, Hui, N, Slusarewicz, P *et al.* (1995). Characterization of a cis-Golgi matrix protein, GM130. *J Cell Biol* **131**(6 Pt 2): 1715–1726.
2. Nakamura, N (2010). Emerging new roles of GM130, a cis-Golgi matrix protein, in higher order cell functions. *J Pharmacol Sci* **112**: 255–264.
3. Puthenveedu, MA, Bachert, C, Puri, S, Lanni, F and Linstedt, AD (2006). GM130 and GRASP65-dependent lateral cisternal fusion allows uniform Golgi-enzyme distribution. *Nat Cell Biol* **8**: 238–248.
4. Diao, A, Frost, L, Morohashi, Y and Lowe, M (2008). Coordination of golgin tethering and SNARE assembly: GM130 binds syntaxin 5 in a p115-regulated manner. *J Biol Chem* **283**: 6957–6967.
5. Vasile, E, Perez, T, Nakamura, N and Krieger, M (2003). Structural integrity of the Golgi is temperature sensitive in conditional-lethal mutants with no detectable GM130. *Traffic* **4**: 254–272.
6. Gozuacik, D and Kimchi, A (2004). Autophagy as a cell death and tumor suppressor mechanism. *Oncogene* **23**: 2891–2906.
7. Qu, X, Yu, J, Bhagat, G, Furuya, N, Hibshoosh, H, Troxel, A *et al.* (2003). Promotion of tumorigenesis by heterozygous disruption of the beclin 1 autophagy gene. *J Clin Invest* **112**: 1809–1820.
8. Arico, S, Petiot, A, Bauvy, C, Dubbelhuis, PF, Meijer, AJ, Codogno, P *et al.* (2001). The tumor suppressor PTEN positively regulates macroautophagy by inhibiting the phosphatidylinositol 3-kinase/protein kinase B pathway. *J Biol Chem* **276**: 35243–35246.
9. Furuta, S, Hidaka, E, Ogata, A, Yokota, S and Kamata, T (2004). Ras is involved in the negative control of autophagy through the class I PI3-kinase. *Oncogene* **23**: 3898–3904.
10. Liang, XH, Jackson, S, Seaman, M, Brown, K, Kempkes, B, Hibshoosh, H *et al.* (1999). Induction of autophagy and inhibition of tumorigenesis by beclin 1. *Nature* **402**: 672–676.
11. Yue, Z, Jin, S, Yang, C, Levine, AJ and Heintz, N (2003). Beclin 1, an autophagy gene essential for early embryonic development, is a haploinsufficient tumor suppressor. *Proc Natl Acad Sci USA* **100**: 15077–15082.
12. Edinger, AL and Thompson, CB (2004). Death by design: apoptosis, necrosis and autophagy. *Curr Opin Cell Biol* **16**: 663–669.
13. Wlodkowic, D, Faley, S, Skommer, J, McGuinness, D and Cooper, JM (2009). Biological implications of polymeric microdevices for live cell assays. *Anal Chem* **81**: 9828–9833.
14. Wlodkowic, D, Skommer, J, McGuinness, D, Hillier, C and Darzynkiewicz, Z (2009). ER-Golgi network–a future target for anti-cancer therapy. *Leuk Res* **33**: 1440–1447.
15. Lowe, SW, Ruley, HE, Jacks, T and Housman, DE (1993). p53-dependent apoptosis modulates the cytotoxicity of anticancer agents. *Cell* **74**: 957–967.
16. Kaufmann, SH and Gores, GJ (2000). Apoptosis in cancer: cause and cure. *Bioessays* **22**: 1007–1017.
17. Ghobrial, IM, Witzig, TE and Adjei, AA (2005). Targeting apoptosis pathways in cancer therapy. *CA Cancer J Clin* **55**: 178–194.
18. Leist, M and Jäättelä, M (2001). Four deaths and a funeral: from caspases to alternative mechanisms. *Nat Rev Mol Cell Biol* **2**: 589–598.
19. Jäättelä, M (2002). Programmed cell death: many ways for cells to die decently. *Ann Med* **34**: 480–488.
20. Okada, H and Mak, TW (2004). Pathways of apoptotic and non-apoptotic death in tumour cells. *Nat Rev Cancer* **4**: 592–603.
21. Levine, B and Yuan, J (2005). Autophagy in cell death: an innocent convict? *J Clin Invest* **115**: 2679–2688.
22. Kroemer, G and Jäättelä, M (2005). Lysosomes and autophagy in cell death control. *Nat Rev Cancer* **5**: 886–897.
23. Maag, RS, Hicks, SW and Machamer, CE (2003). Death from within: apoptosis and the secretory pathway. *Curr Opin Cell Biol* **15**: 456–461.
24. Szegezdi, E, Logue, SE, Gorman, AM and Samali, A (2006). Mediators of endoplasmic reticulum stress-induced apoptosis. *EMBO Rep* **7**: 880–885.
25. Rogan, MT and Richards, KS (1986). Echinococcus granulosus: *in vitro* effect of monensin on the tegument of the protoscolex. *Parasitology* **93 (Pt 2)**: 347–355.
26. Alvarez, C, Garcia-Mata, R, Hauri, HP and Sztul, E (2001). The p115-interactive proteins GM130 and giantin participate in endoplasmic reticulum-Golgi traffic. *J Biol Chem* **276**: 2693–2700.
27. Dennis, JW (1992). *Changes in Glycosylation Associated With Malignant Transformation and Tumor Progression.* CRC Press: Boca Raton. pp. 161–194.
28. Bernales, S, McDonald, KL and Walter, P (2006). Autophagy counterbalances endoplasmic reticulum expansion during the unfolded protein response. *PLoS Biol* **4**: e423.
29. Maiuri, MC, Zalckvar, E, Kimchi, A and Kroemer, G (2007). Self-eating and self-killing: crosstalk between autophagy and apoptosis. *Nat Rev Mol Cell Biol* **8**: 741–752.
30. Baehrecke, EH (2005). Autophagy: dual roles in life and death? *Nat Rev Mol Cell Biol* **6**: 505–510.
31. Chang, SH, Minai-Tehrani, A, Shin, JY, Park, S, Kim, JE, Yu, KN *et al.* (2012). Beclin1-induced autophagy abrogates radioresistance of lung cancer cells by suppressing osteopontin. *J Radiat Res* **53**: 422–432.
32. Chau, YP, Lin, SY, Chen, JH and Tai, MH (2003). Endostatin induces autophagic cell death in EAhy926 human endothelial cells. *Histol Histopathol* **18**: 715–726.
33. Wen, S, Stolarov, J, Myers, MP, Su, JD, Wigler, MH, Tonks, NK *et al.* (2001). PTEN controls tumor-induced angiogenesis. *Proc Natl Acad Sci USA* **98**: 4622–4627.
34. Jiang, HL, Hong, SH, Kim, YK, Islam, MA, Kim, HJ, Choi, YJ *et al.* (2011). Aerosol delivery of spermine-based poly(amino ester)/Akt1 shRNA complexes for lung cancer gene therapy. *Int J Pharm* **420**: 256–265.
35. Singh, RP, Deep, G, Chittezhath, M, Kaur, M, Dwyer-Nield, LD, Malkinson, AM *et al.* (2006). Effect of silibinin on the growth and progression of primary lung tumors in mice. *J Natl Cancer Inst* **98**: 846–855.
36. Cai, KX, Tse, LY, Leung, C, Tam, PK, Xu, R and Sham, MH (2008). Suppression of lung tumor growth and metastasis in mice by adeno-associated virus-mediated expression of vasostatin. *Clin Cancer Res* **14**: 939–949.